ISSN 1063-7761, Journal of Experimental and Theoretical Physics, 2011, Vol. 112, No. 6, pp. 1042–1050. © Pleiades Publishing, Inc., 2011.
Original Russian Text © A.M. Petrzhik, G.A. Ovsyannikov, A.V. Shadrin, K.I. Konstantinyan, A.V. Zaitsev, V.V. Demidov, Yu.V. Kislinskii, 2011, published in Zhurnal Eksperimental'noi i Teoreticheskoi Fiziki, 2011, Vol. 139, No. 6, pp. 1190–1198.

ELECTRONIC PROPERTIES OF SOLID

Electron Transport in Hybrid Superconductor Heterostructures with Manganite Interlayers

A. M. Petrzhik[a,*], G. A. Ovsyannikov[a,b], A. V. Shadrin[a,b], K. I. Konstantinyan[a], A. V. Zaitsev[a], V. V. Demidov[a], and Yu. V. Kislinskii[a]

[a] *Kotelnikov Institute of Radio Engineering and Electronics, Russian Academy of Sciences, Moscow, 125009 Russia*
[b] *Chalmers University of Technology, SE-41296 Göteborg, Sweden*
* *e-mail: petrzhik@hitech.cplire.ru*

Received October 7, 2010

Abstract—Hybrid herostructures comprising an $YBa_2Cu_3O_x$ (YBCO) high-temperature superconductor (HTS) layer and Nb/Au low-temperature superconductor (LTS) bilayer (with critical HTS and LTS temperatures T_c and T'_c, respectively), separated by a thin ($d_M = 5–20$ nm) interlayer of $LaMnO_3$, $La_{0.7}Ca_{0.3}MnO_3$, or $La_{0.7}Sr_{0.3}MnO_3$ manganite have been studied. The electric resistance and magnetic properties of individual (evaporated directly onto the substrate) manganite films and related hybrid herostructures have been measured. Based on quasi-classical equations, analytical expressions for the conductivity of herostructures at $T \leq T'_c$ are obtained in the case of a low-transparency superconductor/manganite interface. It is established that the conductivity of heterostructures is determined by the proximity effect (related to the penetration of a condensate wavefunction from the Nb/Au bilayer to manganite) and depends strongly on interface transparency. At low temperatures ($T \ll T'_c$), the conductivity peaks are found at voltages determined by the exchange field of the manganite interlayer. At $T'_c < T < T_c$, conductivity features at nearly zero bias voltages are observed, which are related to the superconductivity of the YBCO electrode.

DOI: 10.1134/S1063776111050177

1. INTRODUCTION

In recent years, a topical direction in solid state physics that received much attention was related to the interaction of superconductivity and magnetism. This problem was studied in both magnetic superconductors and hybrid structures consisting of superconductors and magnetic materials [1–3]. The so-called proximity effect in these hybrid structures exhibits some nontrivial features, which lead in particular to a nonmonotonic dependence of the critical temperature on the F layer thickness in two-layer superconductor/ferromagnet (S/F) structures. In addition, it is possible to obtain the Josephson π junctions (containing a magnetic material as weak links [3–5]) and to increase the exchange-field-induced critical current in weak links containing two or more F layers [6–8]. The spatially inhomogeneous distribution of the exchange field in a noncollinearly oriented ferromagnet can lead to an anomalous proximity effect as determined by the triplet component of the condensate wavefunction [6]. The effect can also be related to the singlet component of this wavefunction, in which case the proximity effect can be implemented in a multilayer magnetic structure with antiferromagnetic (AF) ordering of magnetization in the layers [9–11].

It should be noted that previous investigations of F/S structures were mostly carried out on polycrystalline films, in which the influence of the crystalline structure of contacting materials was leveled and, hence, some interesting effects could not be observed. For example, the junctions with an AF interlayer did not exhibit an anomalously large proximity effect like that manifested in a magnetic layer structure with an AF-ordered interlayer [10, 11].

This investigation was devoted to hybrid structures containing layers of a magnetic metal, superconducting cuprates, and manganites. Manganites are known to possess an unusual combination of properties [12–15], which account for the special interest in heterostructures with these magnetic materials [16, 17]. These properties include colossal magnetoresistance, crystalline structure type and parameters analogous to those of cuprates, and chemical compatibility with cuprates. Earlier investigations [18–22] showed that thin-layer manganite/cuprate interfaces such as $La_{0.7}Ca_{0.3}MnO_3/YBa_2Cu_3O_x$ (LCMO/YBCO) and $La_{0.7}Sr_{0.3}MnO_3/YBa_2Cu_3O_x$ (LSMO/YBCO) are coherent and free of defects. The chemical diffusion of elements at the interface was absent to within experimental accuracy [21], although more precise measurements [17] revealed manganese ion migration within a range of 1 nm.

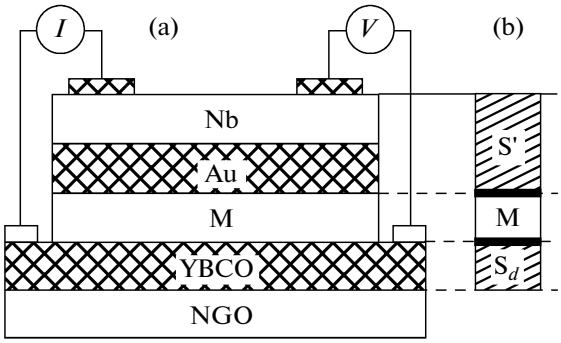

Fig. 1. Schematic diagram of Nb/Au/M/YBCO/NGO hybrid heterostructure: (a) transverse cross section with scheme of current (I) control and response voltage (V) measurement; (b) theoretical model of HHS with allowance for barriers (thick solid lines) at the manganite layer boundaries.

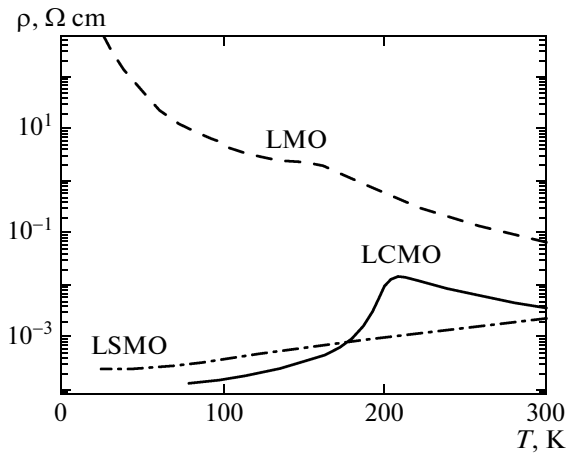

Fig. 2. Temperature dependences of resistivity of the individual manganite films (deposited directly onto substrate).

The above circumstances and a high degree of polarization in manganites make superconductor structures containing these materials interesting model objects for investigating spin-dependent electron transport and proximity effects. In particular, it was established [18, 20] that two-layer LCMO/YBCO structures exhibited a decrease at the superconducting transition temperature if the YBCO layer thickness was below 10 nm, which was explained by the diffusion of spin-polarized carriers. At the same time, the Curie temperature also decreased for an LCMO layer thicknesses below 10 nm [18–22]. Investigations of heterostructures with manganite/cuprate interfaces showed a large variety of electrical properties and gave results that could not be explained using the well-known models [23–25].

This article presents the results of experimental investigations of S'/M/S_d hybrid heterostructures (HHSs) of the Nb/Au/M/YBCO type, where S' is a superconductor with an s-wave symmetry of the order parameter (Nb/Au bilayer) and S_d is an YBCO epilayer possessing predominantly a d-wave symmetry of the order parameter. The magnetically active interlayer (M) was made of either an undoped $LaMnO_3$ (LMO) manganite or optimally doped LCMO and LSMO compositions. The optimum doping level implies an impurity concentration corresponding to the maximum Curie temperature. The data of resistance measurements are compared to the results of calculations using formulas based on the quasi-classical equations of the theory of superconductivity.

2. SAMPLE PREPARATION

Superconducting YBCO cuprate epilayers with a critical temperature of T_c = 88–89 K were manufactured by laser ablation with deposition onto (110)$NdGaO_3$ (NGO) substrates at 700–800°C. Then, a thin interlayer of manganite (M = LMO, LCMO, LSMO) with a thickness of d_M = 5–20 nm was epitaxially grown in the same vacuum chamber at a high temperature and then covered with a thin (20–30 nm) layer of gold (Au) upon cooling to room temperature. A subsequent layer of niobium (Nb) was deposited by magnetron sputtering. The protective Au film reduced the outdiffusion of oxygen from oxides. The proximity effect between the superconducting (Nb) and metal (Au) films determined the critical temperature of the Nb/Au bilayer at T_c' = 8.5–9 K, which was close to the critical temperature (9.2 K) of a pure Nb film. The interlayer of an optimum-doped manganite (M = LCMO, LSMO) at T < 100 K exhibits the properties of a ferromagnetic metal [16, 17]. In the case of undoped manganite (M = LMO), the interlayer at low temperatures must exhibit AF properties [16, 17].

The desired HHS topology was formed using the standard photolithographic, plasmachemical, and ion-beam etching techniques [26]. The cross section of the HHS is a square with side L = 10–50 μm. Figure 1 shows the HHS cross section and the scheme of current control and response voltage measurements.

3. RESULTS OF ELECTRICAL AND MAGNETIC MEASUREMENTS

3.1. Resistance and Magnetic Parameters of Manganite Layers

Since the properties of manganite films are frequently different from those of single crystals (see, e.g., [27]), it is expedient to consider first the temperature dependences (Fig. 2) of the resistance $R(T)$ of individual (evaporated directly onto substrate) manganite films used as interlayers in the HHS. A change in the character of this temperature dependence is indicative of the insulator–metal transition (at T = T_{MI}) at the Curie (T_C) temperature of this magnetic

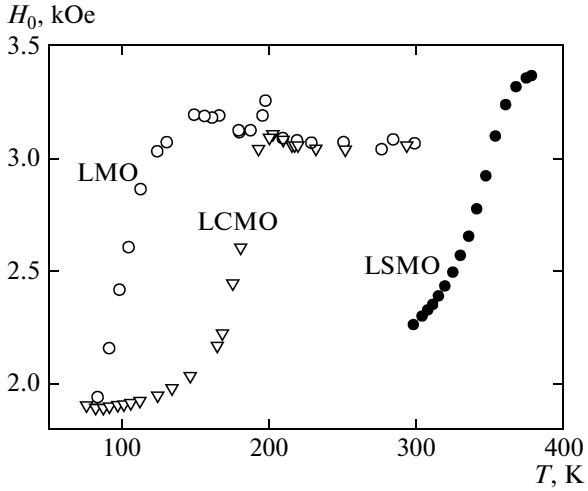

Fig. 3. Temperature dependences of FMR field H_0 (measured at a frequency of 9.76 GHz). for three individual manganite films: (○) LMO; (△) LCMO; (●) LSMO. The Curie temperature T_C was determined at the point of transition from the weak growth (characteristic of a paramagnetic phase) to sharp drop in $H_0(T)$: T_C(LMO) = 150 K; T_C(LCMO) = 200 K; T_C(LSMO) = 370 K.

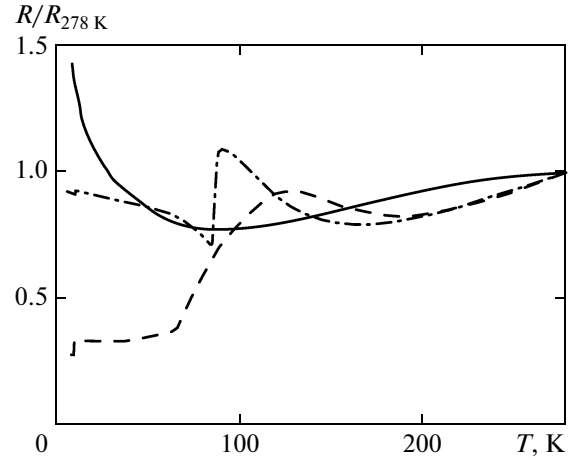

Fig. 4. Temperature dependences of the normalized resistance in HHSs with manganite interlayers of tree types: (dash–dot curve) LMO; (dash curve) LCMO; (solid curve]) LSMO. Local maxims correspond to the metal–insulator transition. $R(T)$ is the resistance at $T = 278$ K.

film. This transition is more clearly pronounced for LCMO at a temperature of $T = 210$ K, above which the conductivity is of the thermoactivated type, while below 210 K it is of the metallic type. For an LSMO film, T_C is above room temperature and occurs outside the temperature interval of measurements; in the undoped LMO film, the metal–insulator transition is not observed and only a small change in the curvature of $R(T)$ plot takes place. The resistivity of an individual LMO film at low temperatures is several orders of magnitude higher than those of LCMO and LSMO.

The Curie temperatures of the individual manganite films and HHSs were determined from the temperature dependences of the ferromagnetic resonance (FMR) field H_0 at a frequency of 9.76 GHz. As the temperature decreases, the FMR field initially exhibits a weak increase (characteristic of a paramagnetic phase), which changes to a sharp drop in $H_0(T)$ on approaching the Curie temperature (Fig. 3). These T_C values were (i) somewhat different from those determined from the measurements of the susceptibility of single-crystalline samples and (ii) strongly dependent on the quality of crystalline films, mechanical stresses, and composition stoichiometry with respect to oxygen [27].

For LCMO and LSMO layers, these T_C values were close to the corresponding metal–insulator transition temperatures as determined from the $R(T)$ curves (Fig. 2). Despite the fact that no bending point characteristic of the metal–insulator transition was observed on the $R(T)$ curves for the undoped LMO films, these films exhibited a paramagnetic–ferromagnetic phase transition. The T_C values determined from the FMR data for LMO films were about 100 K. As is well known, the main factor accounting for the appearance of ferromagnetism in doped manganites is the double exchange between Mn^{3+} and Mn^{4+} ions [28]. In manganites with low doping levels, the appearance of F and AF phases is due to the superexchange between Mn^{3+} ions. An important role in the interactions of these ions is played by the Jahn–Teller distortion [29, 30], as a result of which the F phase exists even in the undoped stoichiometric LMO and nonstoichiometric $LaMnO_{3+\delta}$. The presence of stresses induced by the substrate [27] in LMO epilayers enhances the ferromagnetism analogously to the effect of external pressure [30].

In HHSs with LCMO interlayers, the T_C exhibited a decrease with decreasing d_M below 10 nm. At the same time, an analogous decrease in T_C for the structures with LSMO interlayers was observed at significantly smaller d_M values (below 2 nm), for which the interlayer could become inhomogeneous.

3.2. Temperature Dependences of Resistivity in Hybrid Heterostructures

Figure 4 shows the temperature dependences of the resistivity at low levels of mechanical stresses in HHSs with manganite interlayers of the three types under consideration. At relatively high temperatures ($T >$ 150 K), the behavior of $R(T)$ is determined primarily by the temperature dependence of the resistivity of the YBCO electrode. A small deviation from the linear decrease in $R(T)$ for HHSs with LSMO interlayers is related to their high Curie temperatures ($T_C > 300$ K). A decrease in resistivity observed at $T \leq T_c$ is caused by the superconductivity of YBCO, while the decrease at $T \leq T'_c$ is additionally influenced by superconductivity in the Nb/Au electrode. Note, however, that the

superconducting transition in the Nb/Au electrode for the HHSs with LSMO interlayers is not observed. It is also seen that the contribution from the manganite interlayer and superconductor/manganite interfaces is strongly manifested at temperatures near the metal–insulator transition (T_{MI}), which is close to the Curie temperature. In this case, $R(T)$ and T_{MI} (as well as T_C) depend on the composition of the manganite interlayer. Note that T_{MI} for LCMO is not much higher than the temperature of the superconducting electrode, which accounts for the most rapid variation of $R(T)$ in the vicinity of $T = 100$ K.

A decrease in T_{MI} with the thickness of the manganite interlayer, which was reported earlier (see, e.g., [18, 19]), was also observed in our experiments. For HHSs with LSMO interlayers (possessing high T_C values), the interlayer, as well as the YBCO film, contributes to the $R(T)$ curves at $T > T_c$. At low temperatures, the HHSs with LSMO and LMO (in contrast to LCMO) interlayers exhibit an increase in $R(T)$ with decreasing temperature.

The resistivity of individual LCMO films (deposited directly onto substrates) at $T = 4.2$ K amounted to $\rho_M = 10^{-3}$ Ω cm. The contribution of a manganite interlayer with this resistivity to the characteristic resistance of HHS is expected to be very small ($R_M A = \rho_M d_M = 10^{-9}$ Ω cm^2 at $d_M = 10$ nm). However, the measured characteristic resistance of this HHS ($R_N A \approx 2 \times 10^{-4}$ Ω cm^2 at $d_M = 10$ nm) proved to be much greater than expected. Therefore, the resistance of an HHS with an LCMO interlayer at low temperatures ($T < T_c'$) is determined by the resistances of barriers I_1 and I_2 between the manganite and adjacent layers, while the resistance of the interlayer proper can be ignored.

The opposite situation tales place in the HHS with LMO interlayer, for which the resistance of the individual manganite film increases with decreasing temperature (Fig. 2). For a resistivity of 10^3 Ω cm at $T <$ 10 K (Fig. 2), its contribution to the characteristic resistance of the HHS ($\rho_M = 10^{-2}$ Ω cm^2 at $d_M = 10$ nm) must be significantly greater. However, the experimental value of $R_N A$ of the HHS is lower by several orders of magnitude. Therefore, the resistances of thin LMO films in contact with YBCO exhibit a change by analogy with that reported for $Ca_{0.7}Sr_{0.3}CuO_x$ films [10]. The observed growth in $R_N A$ with increasing $d_M >$ 10 nm (Fig. 5) indicates that the modified layer thickness does not exceed 10 nm.

Taking into account the resistance of the Au/M interface (which was determined in an additional experiment) and the published data [31] and assuming that the interlayer resistance is relatively small, we conclude that the resistance of the M/YBCO interface makes the maximum contribution to the HHS resistance. The (Nb/Au)/M interface also has a low transparency. For this reason, the heterostructures under consideration can be considered $S'–I_1–M–I_2–S_d$ structures, in which the role of barriers I_1 and I_2 is played by the (Nb/Au)/M and M/YBCO interfaces, respectively, while the Nb/Au bilayer is a superconductor with the *s*-wave symmetry of the order parameter in contrast to the S_d (YBCO) superconductor, which predominantly possesses the *d*-wave symmetry of the order parameter. The results of measurements of several characteristic HHS samples at low temperatures are summarized in the table. Note that the R_N values for HHSs were determined at a bias voltage of $V \geq 2$ mV, where the influence of gap peculiarities of the superconducting Nb/Au electrode is minimum.

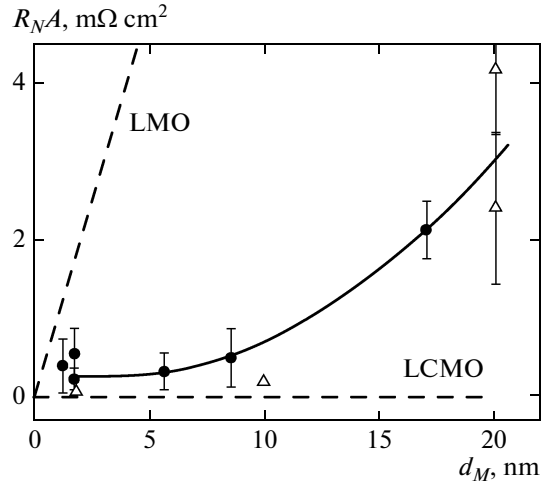

Fig. 5. Plots of the characteristic resistance ($R_N A$) versus interlayer thickness (d_M) for HHSs with interlayers of (●) LMO and (△) LCMO (vertical bars indicate the confidence intervals). Solid curve is the approximation of experimental values; dashed curves show contributions due the resistances of manganite interlayers.

Figure 5 shows the dependence of the characteristic resistance ($R_N A$) versus interlayer thickness (d_M) for HHSs with LMO and LCMO interlayers. The vertical bars indicate the confidence intervals related to the spread of the parameters of five HHSs with different sizes L (see table) manufactured on a common chip. The solid curve shows the approximation of experimental values for the LMO interlayer by a power polynomial; dashed curves show contributions from the resistances of manganite interlayers ($\rho_M d_M$), as calculated using the values of resistivities of the individual LCMO and LMO films at $T = 4.2$ K (see Fig. 2).

3.3. Dependence of HHS Conductivity on Applied Voltage

Figure 6 shows how the voltage dependence of the conductivity $\sigma(V)$ of an HHS with a 10-nm-thick LCMO interlayer varies when the temperature is increased above liquid helium temperature. As can be seen, the conductivity decreases at small voltages and exhibits bending at a voltage corresponding to the superconducting gap of niobium. Pair correlations

Results of resistance measurements for HHSs at $T = 4.2$ K

Structure no.	Interlayer material	L, μm	d_M, nm	$R_N A$, mΩ cm^2	σ_0/σ_N
1	LCMO	30	10	176	0.73
2	LCMO	30	20	3645	0.89
3	LCMO	40	20	1824	0.97*
4	LMO	30	5.6	233	0.9*
5	LSMO	50	1.6	325	0.68

* Measurements at $T = 6$ K.

penetrate from the Nb/Au superconductor into the interlayer and modify the density of states. A superconducting current in the structure is absent up to a temperature of 0.3 K and an interlayer thickness of $d_M = 5$ nm, which can be explained by a negligibly small proximity effect (related to the penetration of a condensate wavefunction from the YBCO layer to manganite). This, in turn, may be caused by the d-wave symmetry of the YBCO condensate wavefunction (or, more precisely, by the negligibly small value of its s-wave component) that penetrates into the M interlayer to a depth equal to the electron mean free path (small compared to the interlayer thickness [32]).

Thus, the conductivity $\sigma(V)$ of the HHS is determined by the proximity effect in the M interlayer, which is related to the penetration of a condensate wavefunction from the Nb/Au superconductor. The nonstoichiometry of the LMO film causes weak ferromagnetism, which leads to a situation analogous to that observed for the HHS with an LCMO interlayer (see Section 3.1).

The appearance of critical current at small values of the interlayer thickness ($d_M < 5$ nm) is related to flaws

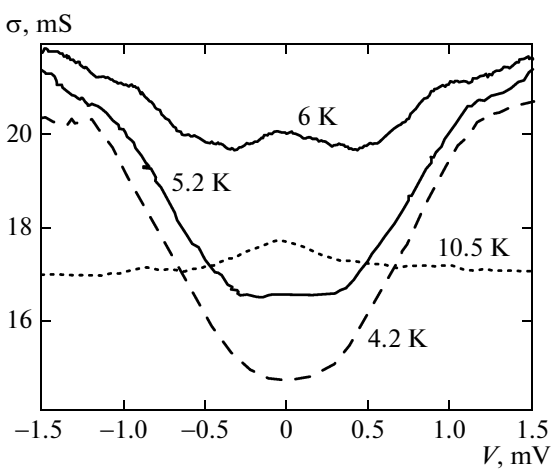

Fig. 6. Family of plots of the conductivity σ versus voltage V for HHS with LCMO interlayer ($d_M = 10$ nm; $L = 30$ μm) measured at various temperatures in the interval of $4.2\ \text{K} < T < 10.5$ K.

appearing in the structure. This leads to the absence of oscillatory dependences of the critical current on the magnetic field and the absence of oscillations on the Shapiro steps (related to the effect of an external electromagnetic field in the millimeter wavelength range). The current–voltage characteristics of the HHSs exhibit features that manifest themselves as an increase in differential resistance.

As the temperature increases to $T \geq 6$ K (Fig. 6), the conductivity $\sigma(V)$ exhibits weak growth in the region of small voltages, which can be related to the proximity effect. This behavior is analyzed in the next section for a particular heterostructure model.

4. THEORETICAL MODEL OF S'–I$_1$–M–I$_2$–N STRUCTURE

Below we assume that conditions in the manganite interlayer admit the diffusion transport of electrons; that is, the electron mean free path l obeys the inequality $l \ll d_M$ for $\xi^* = (v_F l/3\varepsilon^*)^{1/2}$, where v_F is the Fermi velocity, H_{ex} = exchange field in the M interlayer (assumed to be homogeneous and oriented parallel to the interface), d_M is the interlayer thickness, and $\varepsilon^* = \max(T, \Delta', H_{ex})$ is the characteristic energy. For the d-wave symmetry of the order parameter in the YBCO layer, the condensate wavefunction penetrates from the YBCO layer into the manganite to a depth (on the order of l) that is small compared to the interlayer thickness, so that the influence of the superconducting pairing in YBCO on the proximity effect in the interlayer can be ignored. Because of this, in analyzing the transport phenomena and proximity effect in the system, we will consider a model where the YBCO layer is replaced by a normal metal (N).

For a collinear orientation of the exchange field in the ferromagnetic layer, calculations analogous to those carried out in [33] lead to the following expression for the current (in units of $k = \hbar = 1$):

$$I = \frac{1}{8eR_N}\int d\varepsilon[J_+(\varepsilon) + J_-(\varepsilon)] \times \left[\tanh\left(\frac{\varepsilon + eV}{2T}\right) - \tanh\left(\frac{\varepsilon - eV}{2T}\right)\right], \quad (1)$$

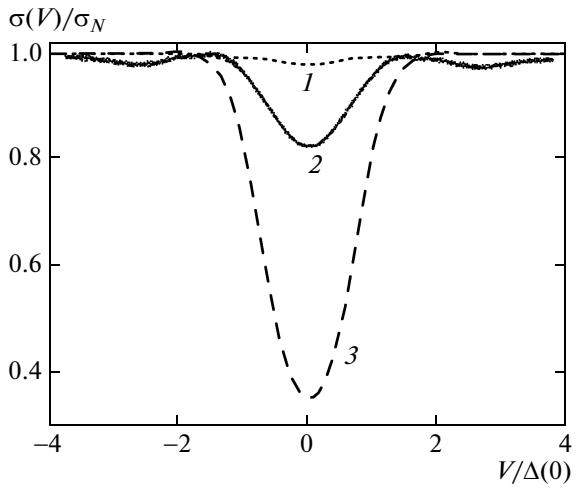

Fig. 7. Family of voltage dependences of the conductivity calculated for the S'–I_1–M–I_2–N structure at $\varepsilon_{b1}/\Delta' = 10^{-1}$ (*1*), 10^{-2} (*2*), and 10^{-3} (*3*) (dashed curves *1–3*, respectively) for a normalized exchange energy of $H_{ex}/\Delta' = 2$, and $T'_c = 9$ K. The solid curve represents the experimental data for an HHS with 10-nm-thick LCMO interface.

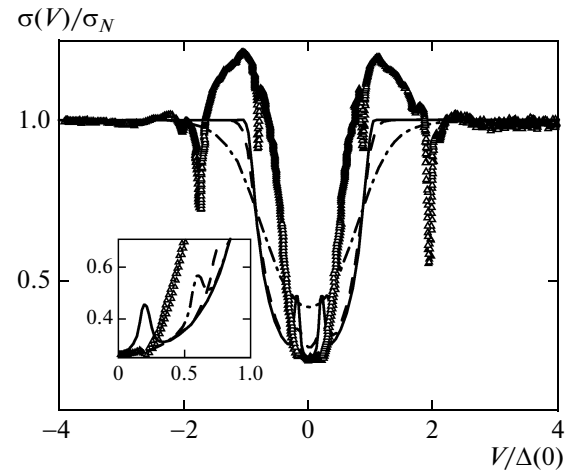

Fig. 8. Theoretical voltage dependences of the conductivity calculated for the S'–I_1–M–I_2–N structure at various temperatures: $T = 0.3$ K (solid curve); 1 K (dashed curve); 4.2 K (dash–dot curve). Points (△) represent the experimental data for 40 × 40 μm^2 HHS with a 20-nm-thick LCMO interface. Theoretical curves are constructed for $r_{b1} = 2.8 \times 10^{-3}$; $\gamma/\Delta'(0) = 10^{-3}$ (parameter γ characterizes inelastic processes in S'), $H_{ex} = 0.2\Delta'(0)$. The inset shows the transformation of theoretical $\sigma(V)$ curves depending on the exchange energy, $H_{ex} = 0.2\Delta'(0)$ (solid curve); 0.6 (dash–dot curve); 0.75 (dashed curve), in comparison to the experimental data (△) for $r_{b1} = 2.8 \times 10^{-3}$ and $t = T/T'_c = 0.3$.

where

$$J_\mu(\varepsilon) = \frac{1}{Q_{1\mu}(\varepsilon) + Q_{2\mu}(\varepsilon) + r_M q_\mu(\varepsilon)},$$

$$Q_{2\mu}(\varepsilon) = r_{b2}\frac{1}{\mathrm{Re}g^R(\varepsilon + \mu H_{ex}, 0)},$$

$$Q_{1\mu}(\varepsilon) = r_{b1}\frac{1}{M_\mu(\varepsilon)}, \quad r_{b1,2} = \frac{R_{b1,2}}{R_N},$$

$$r_M = \frac{R_M}{R_N}, \tag{2}$$

$$M_\mu(\varepsilon) = \mathrm{Re}g^R(\varepsilon + \mu H_{ex}, d_M)\mathrm{Re}g^R_{S'}(\varepsilon)$$

$$+ \mathrm{Im}f^R(\varepsilon + \mu H_{ex}, d_M)\mathrm{Im}f^R_{S'}(\varepsilon),$$

$$q_\mu(\varepsilon) = \frac{1}{d_M}\int_0^{d_M} dx \frac{1}{\cosh^2(\mathrm{Re}\theta_\mu)}.$$

Here, $R_N = R_{b1} + R_{b2} + R_M$ is the resistance of the structure in the normal state, R_M is the resistance of the M interlayer, $\mu = \pm$ and θ_μ is determined as

$$\cosh\theta_\mu = g^R(\varepsilon + \mu H_{ex}, x).$$

We also assume that the transparency of barriers I_1 and I_2 is small compared to unity (the case of arbitrary transparencies is considered below). In the case of a thin M interlayer (i.e., under the condition that $d_M \ll \xi^*$), the Green's functions are given by the following expressions:

$$g^E(\varepsilon) = \frac{\varepsilon + i(\varepsilon_{b2} + \varepsilon_{b1}g^R_{S'})}{\{[\varepsilon + i(\varepsilon_{b2} + \varepsilon_{b1}g^R_{S'}(\varepsilon))]^2 + (\varepsilon_{b1}f^R_{S'}(\varepsilon))^2\}^{1/2}},$$

$$f^R(\varepsilon) = \frac{i\varepsilon_{b1}f^R_S(\varepsilon)}{\{[\varepsilon + i(\varepsilon_{b2} + \varepsilon_{b1}g^R_{S'}(\varepsilon))]^2 + (\varepsilon_{b1}f^R_{S'}(\varepsilon))^2\}^{1/2}}, \tag{3}$$

where $\varepsilon_{bj} = D_{bj}v_F/4d_M$ ($j = 1, 2$) and D_{bj} is the averaged transparency of the corresponding barrier.

In the case where the resistances of the barriers predominate, we have

$$F_\mu(\varepsilon) = \frac{M_\mu(\varepsilon)\eta_\mu(\varepsilon)}{r_{b2}M_\mu(\varepsilon) + r_{b1}\eta_\mu(\varepsilon)}. \tag{4}$$

The results of numerical calculation of the dependence of conductivity in the S'–I_1–M–I_2–N' heterostructure on the voltage are presented in Figs. 7 and 8.

5. COMPARISON TO EXPERIMENT

As can be seen from an analysis of the data presented in Fig. 6, the $\sigma(V)$ curve at $T \geq T'_c$ exhibits features that are most probably related to the influence of

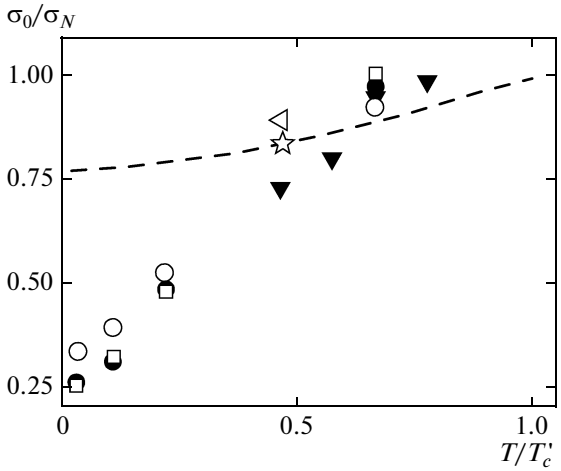

Fig. 9. Experimental plot of the conductivity of HHS (LCMO interlayer) with a linear size of 10, 20, 30, 40, and 50 μm at zero bias voltage versus temperature (points). The dashed curve shows the theoretical dependence calculated for $r_{b1} = 3 \times 10^{-3}$ and $\gamma = 0.01$.

the S_d superconductor. On the other hand, features in the behavior of $\sigma(V)$ at lower temperatures are primarily related to the proximity effect caused by the penetration of a condensate wavefunction from the S' superconductor to the manganite interlayer. Note that qualitatively (not considering features die to the proximity effect), the shape of $\sigma(V)$ at $T = 4.2$ K corresponds to that typical of the S'–I–N tunneling junctions, which are characterized by minimum conductivity at low voltages and an increase in σ at $V \approx \Delta'/e$ (where Δ' is the superconducting gap). As was noted above, the c axis of YBCO in the HHSs under consideration is oriented perpendicularly to the interfaces. In this case, no Andreev bound states appear at the $M(N)/S_d$ interface (see, e.g. [34]) and, hence, there are no features related to these states (as were studied, e.g., in [12, 13, 34]).

In addition to features in the density of states at the energies $\varepsilon \approx \Delta'$, the structure exhibits features at $\varepsilon \approx \varepsilon_{b1} = \hbar D_2 v_F/4d_M$. Figure 7 shows the experimental plot of $\sigma(V)$ (normalized to the asymptotic value of conductivity) in comparison to the results of numerical calculations for the $S'–I_1–M–I_2–N$ structure at several values of the parameter $\varepsilon_{b2}/\Delta'(0)$, where $\Delta'(0)$ is the order parameter in the Nb/Au bilayer at $T = 0$). As can be seen, the best agreement of theory and experiment is achieved for $\varepsilon_{b2}/\Delta'(0) = 0.01$. Note that the variation of H_{ex} within $(1–10)\Delta'(0)$ does not change the shape of the curve at normalized temperatures $t = T/T'_c \geq 0.4$.

Since barrier transparency D at the interface is determined by its resistance R_bA (see, e.g., [35]), we have

$$D \approx \rho l/R_bA, \quad (5)$$

where ρ and l are the resistivity and mean free path, respectively, of the manganite interlayer. Thus, the transparencies of the two barriers are connected via the relation for the total resistance of the HHS, defined as $R_N = R_{b1} + R_{b2}$. For $\rho(\text{LCMO}) = 0.1$ mΩ cm, $l = 10$ nm, and $R_NA \approx 2 \times 10^{-4}$ Ω cm^2, formula (5) yields $D \approx 3 \times 10^{-7}$ at liquid helium temperature ($T = 4.2$ K) [29]. As a result, ε_{b2} can be estimated at 1.4×10^{-6}, which significantly differs from the estimate obtained by superimposing a theoretical curve onto the experimental data ($\varepsilon_{b2} \sim 10^{-2}$, Fig. 7). However, according to independent measurement results [31], the characteristic resistance of the LSMO/Au interface is significantly smaller ($R_NA = 8 \times 10^{-7}$ Ω cm^2). Therefore, the system under consideration exhibits a significant asymmetry in the transparencies of interfaces. Using data from [31] for estimating the parameters of the LSMO/Au interface, we obtain $\varepsilon_{b2} \sim 3.6 \times 10^{-4}$, which is somewhat closer to the estimate obtained from analysis of Fig. 7.

The situation significantly changes when the temperature is decreased to $t = T/T'_c < 0.3$. This leads to a sharp decrease in $\sigma(0) = \sigma_0$ and, as a result, $\sigma(V)$ exhibits some features that are independent of the temperature (Fig. 8). The features observed at low voltages vary depending on the exchange field H_{ex}. The best agreement between theory and experiment for HHSs with 10-nm-thick LCMO interlayers is observed for $H_{ex} = 10^{-2}\Delta'(0)$. This value is somewhat smaller than the simple estimate of the exchange field at $H_{ex} = T_C/10$ for $T_C \approx 120$ K (conditionally determined for the metal–insulator transition in the HHS, Fig. 4).

The experimental data reveal some features at voltages in the vicinity of the S' superconductor gap that are absent in our calculation results. It cannot be excluded that these features are due to the magnetically active nature of the barriers formed at the interfaces. Calculations performed in Section 4 did not take into account the variation of properties of the barriers under the action of the magnetic field.

Figure 9 shows the temperature dependence of the HHS conductivity σ_0 at a zero bias voltage. As can be seen, the temperature dependence of σ_0 at high temperatures $t > 0.5$ agrees with the results of calculations performed for the parameters taken from the data in Fig. 7. The same range of temperatures is characterized by a small influence of the exchange field on σ_0. At relatively low temperatures, $t < 0.4$, $\sigma_0(T)$ exhibits a significant decrease that is not described by the proposed theoretical model (4) with the experimental values of the HHS parameters. This discrepancy is probably also related to the magnetically active nature of

the barriers formed at the interfaces, which was not taken into account in the model considerations in Section 4.

6. CONCLUSIONS

A comparison of the data of experimental investigations of HHSs based on cuprate (YBCO) and low-temperature superconductors separated by thin manganite interlayers, on the one hand, and the results of theoretical calculations performed using quasi-classical equations of the theory of superconductivity, on the other hand, showed the presence of features in the voltage dependence of the conductivity that are related to the proximity effect. In our experiments, the primary influence is due to the proximity effect, related to the penetration of a condensate wavefunction from the low-temperature superconducting Au/Nb electrode into the manganite interlayer. Deviations of the conductivity of heterostructures from the results of model calculations is most likely related to the magnetically active nature of the barriers formed at the interfaces between the manganite interlayer and superconducting electrodes.

ACKNOWLEDGMENTS

The authors are grateful to T. Bauch, I.V. Borisenko, D. Winkler, A.V. Kalabukhov, and I.M. Kotelyanskii for fruitful discussions of results and assistance in performing investigations.

This study was supported in part by the Department of Physical Sciences of the Presidium of the Russian Academy of Sciences, the Ministry of Education and Science of the Russian Federation (project no. 02.740.11.0795), the Russian Foundation for Basic Research (project no. 08-02-00487), the International Science and Technology Center (grant no. 3743), and the Presidential Grant for Support of Scientific Schools in Russia (project no. NSh-5423.2010/2).

REFERENCES

1. A. Buzdin, Rev. Mod. Phys. **77**, 935 (2005).
2. F. S. Bergeret, A. F. Volkov, and K. B. Efetov, Rev. Mod. Phys. **77**, 1321 (2005).
3. A. A. Golubov, M. Yu. Kupriyanov, and E. Il'ichev, Rev. Mod. Phys. **76**, 411 (2004).
4. L. N. Bulaevskii, V. V. Kizii, and A. A. Sobyanin, Pis'ma Zh. Eksp. Teor. Fiz. **25** (7), 314 (1977) [JETP Lett. **25** (7), 290 (1977)].
5. V. V. Ryazanov, V. A. Oboznov, A. V. Veretennikov, A. Yu. Rusanov, A. A. Golubov, and J. Aarts, Phys. Rev. Lett. **86**, 2426 (2001).
6. F. S. Bergeret, A. F. Volkov, and K. B. Efetov, Phys. Rev. Lett. **86**, 3140 (2001).
7. Yu. S. Barash and I. V. Bobkova, Phys. Rev. B: Condens. Matter **65**, 144502 (2002).
8. A. V. Zaitsev, Pis'ma Zh. Eksp. Teor. Fiz. **83** (6), 277 (2006) [JETP Lett. **83** (6), 233 (2006)]; Pis'ma Zh. Eksp. Teor. Fiz. **88** (7), 521 (2008) [JETP Lett. **88** (7), 448 (2008)].
9. A. V. Zaitsev, Pis'ma Zh. Eksp. Teor. Fiz. **90** (6), 521 (2009) [JETP Lett. **90** (6), 475 (2009)].
10. A. V. Zaitsev, G. A. Ovsyannikov, K. Y. Constantinian, Yu. V. Kislinskii, A. V. Shadrin, I. V. Borisenko, and P. V. Komissinskiy, Zh. Eksp. Teor. Fiz. **137** (2), 380 (2010) [JETP **110** (2), 336 (2010)].
11. L. Gor'kov and V. Kresin, Appl. Phys. Lett. **78**, 3657 (2001).
12. M. Zareyan, W. Belzig, and Yu. V. Nazarov, Phys. Rev. B: Condens. Matter **65**, 184505-1-9 (2002).
13. T. Yokoyama, Y. Tanaka, and A. A. Golubov, Phys. Rev. B: Condens. Matter **73**, 094501 (2006).
14. A. Cottet and W. Belzig, Phys. Rev. B: Condens. Matter **72**, 180503 (2005).
15. SanGiorgio, S. Reymond, M. R. Beasley, J. H. Kwon, and K. Char, Phys. Rev. Lett. **100**, 237002 (2008).
16. K. Dorr, J. Phys. D: Appl. Phys. **39**, R125 (2006).
17. M. B. Salamon and M. Jaime, Rev. Mod. Phys. **73**, 583 (2001).
18. M. Varela, A. R. Lupini, S. Pennycook, Z. Sefrioui, and J. Santamaria, Solid-State Electron. **47**, 2245 (2003).
19. V. Peña, C. Visani, J. Garcia-Barriocanal, D. Arias, Z. Sefrioui, C. Leon, J. Santamaria, and C. A. Almasan, Phys. Rev. B: Condens. Matter **73**, 104513 (2006).
20. O. Moran, E. Bacab, and F. A. Perez, Microelectron. J. **39**, 556 (2008).
21. S. Stadler, Y. U. Idzerda, Z. Chen, S. B. Ogale, and T. Venkatesan, Appl. Phys. Lett. **75**, 3384 (1999).
22. V. Peña, Z. Sefrioui, D. Arias, C. Leon, J. Santamaria, M. Varela, S. J. Pennycook, and J. L. Martinez, Phys. Rev. B: Condens. Matter **69**, 224502 (2004).
23. P. A. Kraus, A. Bhattacharya, and A. M. Goldman, Phys. Rev. B: Condens. Matter **64**, 220505 (2001).
24. Z. Y. Chen, A. Biswas, I. Žutić, T. Wu, S. B. Ogale, R. L. Greene, and T. Venkatesan, Phys. Rev. B: Condens. Matter **63** (21), 212508 (2001).
25. A. Tiwari and K. P. Rajeev, Phys. Rev. B: Condens. Matter **60**, 10591 (1999).
26. P. Komissinskiy, G. A. Ovsyannikov, I. V. Borisenko, Yu. V. Kislinskii, K. Y. Constantinian, A. V. Zaitsev, and D. Winkler, Phys. Rev. Lett. **99**, 017004 (2007).
27. G. A. Ovsyannikov, A. M. Petrzhik, I. V. Borisenko, A. A. Klimov, Yu. A. Ignatov, V. V. Demidov, and S. A. Nikitov, Zh. Eksp. Teor. Fiz. **135** (1), 56 (2009) [JETP **108** (1), 48 (2009)].
28. Yu. A. Izyumov and Yu. N. Scryabin, Usp. Fiz. Nauk **171** (2), 121 (2001) [Phys.—Usp. **44** (2), 109 (2001)].
29. Q. Huang, A. Santoro, J. W. Lynn, R. W. Erwin, J. A. Borchers, J. L. Peng, and R. L. Greene, Phys. Rev. B: Condens. Matter **55**, 14987 (1997).

30. I. M. Fita, R. Szymczak, M. B. Baran, V. Markovich, R. Puzniak, A. Wisniewski, S. V. Shiryaev, V. N. Varyukhin, and H. Szymczak, Phys. Rev. B: Condens. Matter **68**, 014436 (2003).

31. L. Mieville, D. Worledge, T. H. Geballe, R. Contreras, and K. Char, Appl. Phys. Lett. **73**, 1736 (1998).

32. S. Kashiwaya and Y. Tanaka, Rep. Prog. Phys. **63**, 1641 (2000).

33. A. F. Volkov, A. V. Zaitsev, and T. M. Klapwijk, Physica C (Amsterdam) **210**, 21 (1993).

34. F. V. Komissinski, G. A. Ovsyannikov, Yu. V. Kislinskii, I. M. Kotelyanskii, and Z. G. Ivanov, Zh. Eksp. Teor. Fiz. **122** (6), 1247 (2002) [JETP **95** (6), 1074 (2002)].

35. P. V. Komissinskiy, G. A. Ovsyannikov, K. Y. Constantinian, Y. V. Kislinski, I. V. Borisenko, I. I. Soloviev, V. K. Kornev, E. Goldobin, and D. Winkler, Phys. Rev. B: Condens. Matter **78**, 024501 (2008).

36. E. Zhao, T. Löfwander, and J. A. Sauls, Phys. Rev. B: Condens. Matter **70**, 134510 (2004).

Translated by P. Pozdeev